# MEASUREMENTS OF THE RADIATION ENERGY DISTRIBUTION IN THE SOFT X-RAY REGION IN THE WENDELSTEIN VII-A STELLARATOR

A. Weller

IPP 2/277 October 1985

MAX-PLANCK-INSTITUT FÜR PLASMAPHYSIK

8046 GARCHING BEI MÜNCHEN

**MAX-PLANCK-INSTITUT FÜR PLASMAPHYSIK**
**Garching bei München**

# MEASUREMENTS OF THE RADIATION ENERGY DISTRIBUTION IN THE SOFT X-RAY REGION IN THE WENDELSTEIN VII-A STELLARATOR

A. Weller

IPP 2/277 October 1985

*Die nachstehende Arbeit wurde im Rahmen des Vertrages zwischen dem Max-Planck-Institut für Plasmaphysik und der Europäischen Atomgemeinschaft über die Zusammenarbeit auf dem Gebiet der Plasmaphysik durchgeführt.*

# MEASUREMENTS OF THE RADIATION ENERGY DISTRIBUTION IN THE SOFT X-RAY REGION IN THE WENDELSTEIN VII-A STELLARATOR

A. Weller

Max-Planck-Institut für Plasmaphysik,
Association EURATOM-IPP,
Garching bei München,
Federal Republic of Germany

**Abstract**

The soft X-ray radiation power with 400 $eV \leq E \leq 1000$ $eV$ originating from resonance lines of C-, O-, Fe-, Cr-, Mo-impurities contributes the major part of the total radiation losses from the plasma centre. A coarse discrimination between the most important impurity species can be obtained by using an array of filters consisting of different material. Different energy windows are defined by the energies of the corresponding L-line absorption edges of the filter materials. The radiation power of each energy band is monitored by a set of surface barrier diodes during the plasma discharges.

Information about the energy spectrum is also provided by a two filter method giving an estimation of the mean radiation energy. In addition, X-ray pulse height analysis measurements are presented. The results are correlated with spectroscopic measurements.

## CONTENTS

1. Introduction

2. Filter Methods

2.1. L-line absorption edge filters

2.1.1. Experimental method

2.1.2. Performance measurements

2.1.3. Results for neutral beam heated plasmas

2.2. Mean energy from two filter measurements

3. X-ray pulse height analysis

4. Summary

## 1. Introduction

For typical plasmas in Wendelstein VII-A ($R = 200\ cm$, $a = 10\ cm$, l=2, m=5 helical windings), heated exclusively by neutral beams (27 $kV$, $H^0$ *or* $D^0$ , 3-4 beam lines each with a power of $100 - 150\ kW$, almost perpendicular injection ($6^o$)), large centrally peaked radiation losses are measured [1-4]. In the plasma centre, most of the radiation intensity from impurity resonance lines is emitted in the soft X-ray region with $400\ eV \leq E \leq 1000\ eV$. Spectroscopic measurements with a crystal spectrometer is the most appropriate way to monitor the intensity of individual resonance lines. But, it is difficult to get a complete survey of the spectral intensity distribution in this energy range since a wavelength scan with the flat crystal spectrometers at WVII-A can be only made shot by shot. In the region $\sim 20 - 100\ \AA$ also a grazing incidence spectrometer was employed, but it was not available during most of the time. Therefore, also attenuation measurements with different soft X-ray filters and silicon surface barrier detectors were performed. In addition also pulse height analysis (PHA) was applied. Both methods can provide data with an only moderate energy resolution not allowing to resolve single resonance lines. However, these measurements can define a region of interest for more detailed investigations with the crystal spectrometer and also in special cases they can provide a discrimination between different impuritiy species. An advantage of the filter methods is the fast response of the detectors (good time resolution) and the relatively simple way to obtain absolute radiation intensities. In the case of the PHA, the time resolution is poor and a large number of shots is necessary to obtain good statistics of the data but the spectral range which is covered by the measurements is comparitively large.

## 2. Filter Methods

### 2.1. L-LINE ABSORPTION EDGE FILTERS

#### 2.1.1 EXPERIMENTAL METHOD

Absorption edge filters make use of the characteristic step of the mass absorption cross section around the excitation energy of inner shell electrons. They allow to detect the radiation intensity within an energy band defined by the energy gap between the absorption edges of different absorber foils made from adjacent elements

in the periodic system. The thicknesses of the filters have to be matched such that identical transmission curves outside the interesting energy band are achieved.

K-edge filter systems known as Ross-filters have been widely used [5-7] mainly to detect X-radiation in the several keV energy region from short radiation pulses which cannot be investigated with conventional spectrometers. Because of the relatively high K-edge energies of suitable metals, the filters are easy to fabricate since they do not need to to be extremely thin.

In the sub-keV region, however, $L_\alpha$-edge filters of medium Z elements are more suitable, but they have to be very thin in order to keep the transmitted radiation power above the limit of detection.

For the use on the Wendelstein VII-A stellarator a multichannel Ross filter system for the X-ray spectral energy range 400 $eV \leq E \leq 1000$ $eV$ was installed. Ten different elements were chosen consisting of metals with $21 \leq Z \leq 30$ (Sc, Ti, V, Cr, Mn, Fe, Co, Ni, Cu, Zn) which were evaporated on carbon foils of $\sim 15\ \mu g\, cm^{-2}$ thickness. The thickness of the metallized layers varies between $\sim 110\ \mu g\, cm^{-2}$ for Sc and $\sim 42\ \mu g\, cm^{-2}$ for Zn. The ten different transmission curves calculated with the cross section data given in [8,9] including the absorption of the carbon backing and the Al entrance window of the silicon surface barrier detectors are shown in fig. 1a. With the set of thicknesses chosen (given on the right of fig. 1a) the curves perfectly coincide below 400 $eV$ and above 1200 $eV$. The small second step appearing in each of the curves is caused by $L_\beta$-excitation. It can lead to a small but still negligible mixing of adjacent energy bands.

The "spectrometer" response function which can be derived from the differences between each two adjacent transmission curves is plotted in fig. 1b. The spectral energy resolution corresponding to the nine resulting energy channels (covering the energy range from $\sim 400$ $eV$ to $\sim 1030$ $eV$) varies between $\sim 50$ $eV$ and $\sim 90$ $eV$. This is at least a factor of two better compared with the energy resolution of a Si(Li)-diode.

The experimental set up consists of an array of 10 rectangular surface barrier diodes with 40 $\mu g\, cm^{-2}$ Al entrance window (same detector type as used for the soft X-ray camera at WVII-A [4,10,11]. All the diodes view the entire central plasma region (same solid angle, no spatial resolution). In front of each diode one of the filters can be mounted.

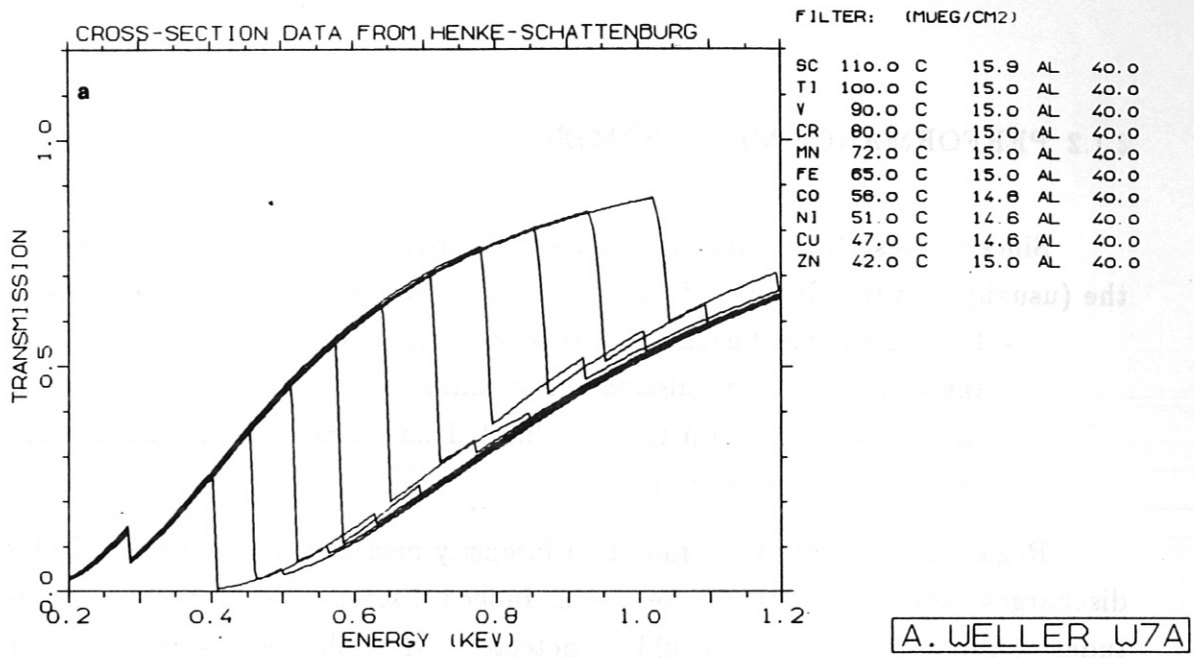


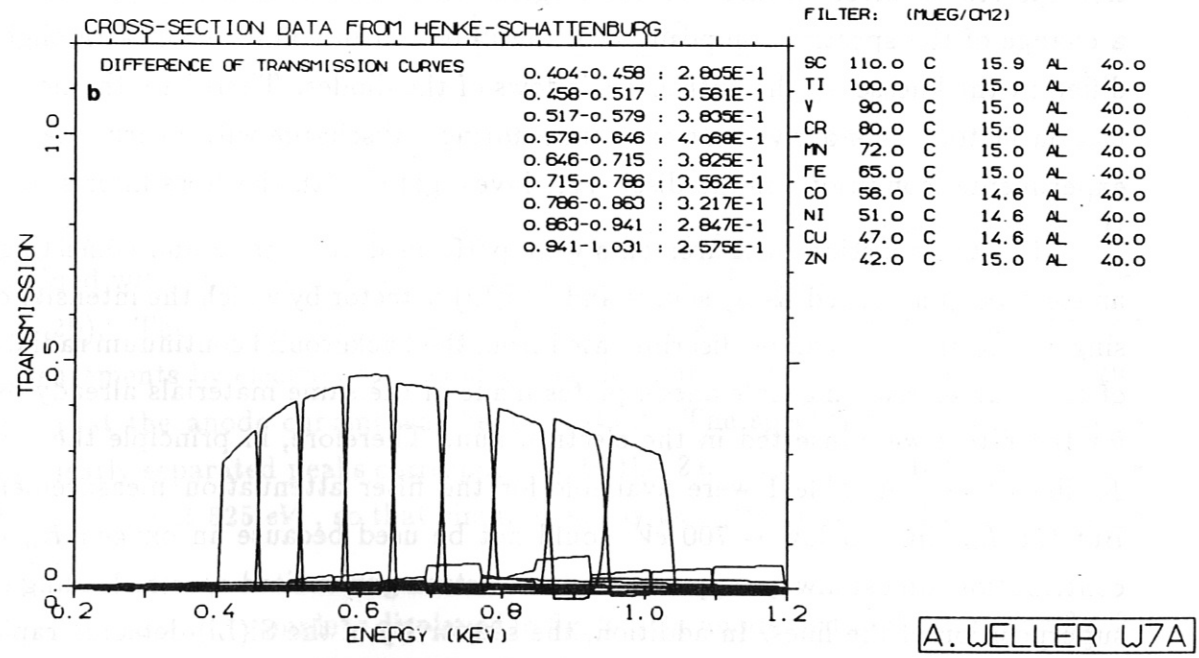


Fig. 1 a) Calculated filter transmission curves for elements between Sc and Zn (matched thicknesses) including absorption in layers of C (backing) and Al (electrode of surface barrier diodes).

b) Differences of adjacent curves in a) defining the response functions of the spectrometer channels.

### 2.1.2 PERFORMANCE MEASUREMENTS

Since the resulting radiation powers of different energy bands are derived from the (usually small) difference of two signals it is desirable to check experimentally

- the sensitivity of each diode relative to each other
- the calculated transmission curves since the accuracy of the thickness of the evaporated metal layers is limited and also errors in the absorption cross sections may occur.

Regarding the first item, radiation intensity measurements for typical plasma discharges were made without the filters. Indeed discrepancies in the signal amplitudes of the order of $\sim 5\%$ could be detected. Multiplication factors which normalize all the signals of the different channels (without filter) to same amplitudes were derived from the measurements. In addition, small changes of the normalization factors occurred during the discharges. This effect is probably produced by a change of the spectral composition of the radiation in combination with slightly different thicknesses of the entrance windows of the diodes. Therefore, the normalization factors were derived for each time during a discharge with nearly the same experimental conditions as the discharges investigated with the Ross filter system.

The transmission measurements were performed at a test stand consisting of an electron gun excited X-ray source and a Si(Li) detector by which the intensity of a single resonance line can be discriminated from the background continuum radiation of the source. Exchangeable anode plates made of the same materials already used for the filters were inserted in the electron gun. Therefore, in principle the set of $L_\alpha$-lines listed in table I were available for the filter attenuation measurements. But the $L_\alpha$ lines below $\sim 700\ eV$ could not be used because an oxygen $K_\alpha$-line contribution almost always appeared in the electron gun excited spectra leading to a superposition of the lines. In addition, the sensitivity of the Si(Li)-detector rapidly decreases in the low energy region. But in the case of a clear separation the $O - K_\alpha$ line also provides additional data points at $525\ eV$.

Table I

Electron gun excited lines
used for filter transmission measurements

| Line | Energy [eV] |
|---|---|
| Ti – $L_\alpha$ [a] | 452 |
| V – $L_\alpha$ [a] | 511 |
| O – $K_\alpha$ | 525 |
| Cr – $L_\alpha$ [a] | 573 |
| Mn – $L_\alpha$ [a] | 637 |
| Fe – $L_\alpha$ [a] | 705 |
| Co – $L_\alpha$ | 776 |
| Ni – $L_\alpha$ | 851 |
| Cu – $L_\alpha$ | 930 |
| Zn – $L_\alpha$ | 1012 |
| O – $K_\alpha$ | 525 |

[a] blended by O – $K_\alpha$ or in low energy cut-off

As an example for the measurements, fig. 2 gives the pulse height spectra obtained with an Zn-anode without filter (fig. 2a) and with a 47 $\mu g\, cm^{-2}$ Cu-filter (fig. 2b). The emissivity of the X-ray source was kept constant during the two measurements by electronically controlling the filament current of the electron gun such that the anode current was kept constant. The spectra of figs. 2a,b contain two clearly separated peaks corresponding to the $Zn - L_\alpha$ line at 1012 $eV$ and the $O - K_\alpha$ line at 525 $eV$ , so that simultaneously two attenuation data points can be obtained.

The second example is displayed in fig. 2c (Cu-anode, without filter) and fig. 2d (with 90.0 $\mu g\, cm^{-2}$ V-filter). Since the $V - L_\alpha$ absorption edge has a lower energy (517 $eV$) than the $O - K_\alpha$ line (525 $eV$), the oxygen peak completely vanishes with the vanadium filter.

In fig. 3 all the measured transmission data points (except for Sc) are compiled together with the calculated curves. Within the error bars the overall agreement is very satisfactory so that the filter system should be useful to obtain spectroscopic information.

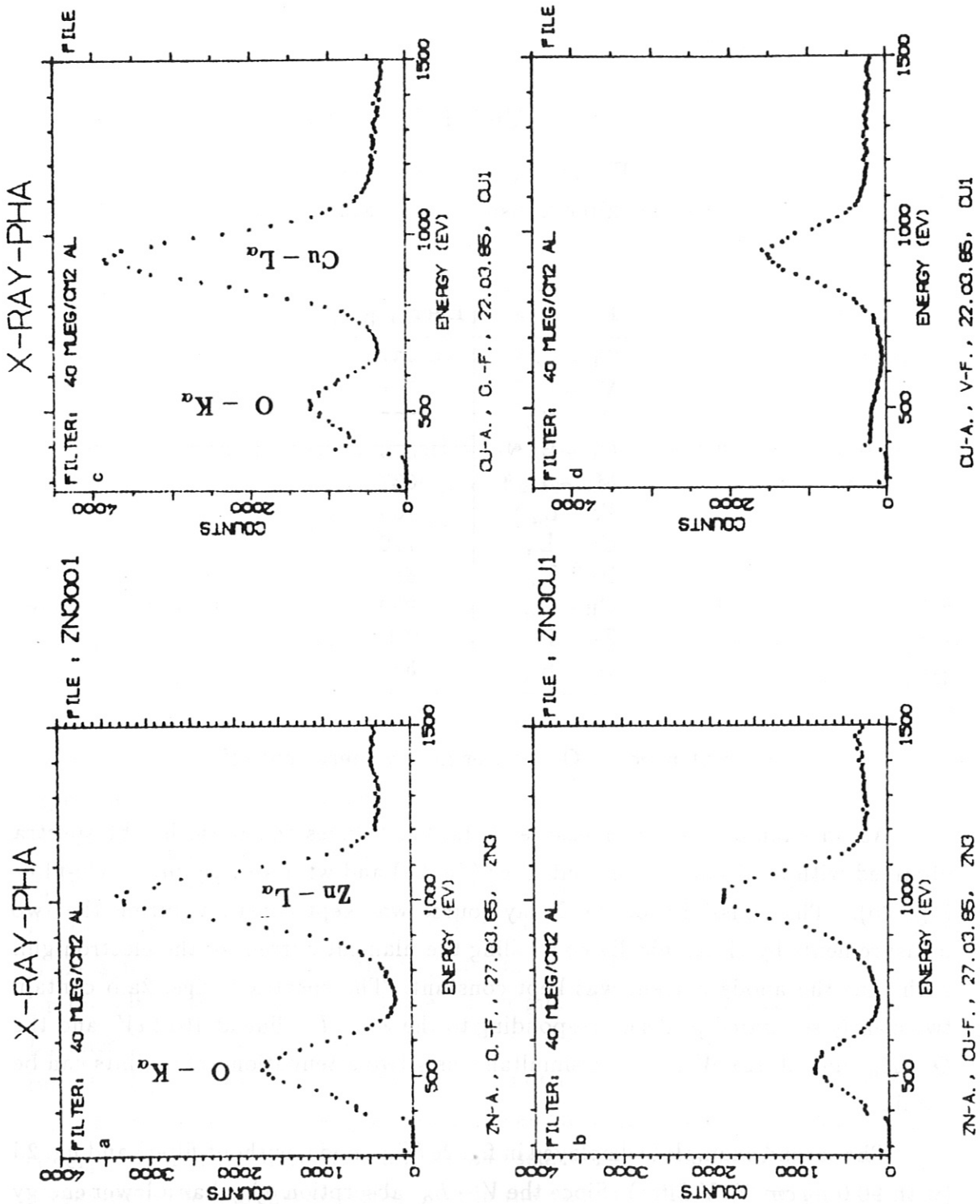


Fig. 2 Pulse height spectra obtained during filter transmission measurements:

a) Zn-Anode, no filter.

b) Zn-Anode, with Cu-filter (47 $\mu g\, cm^{-2}$).

c) Cu-Anode, no filter.

d) Cu-Anode, with V-filter (90 $\mu g\, cm^{-2}$).

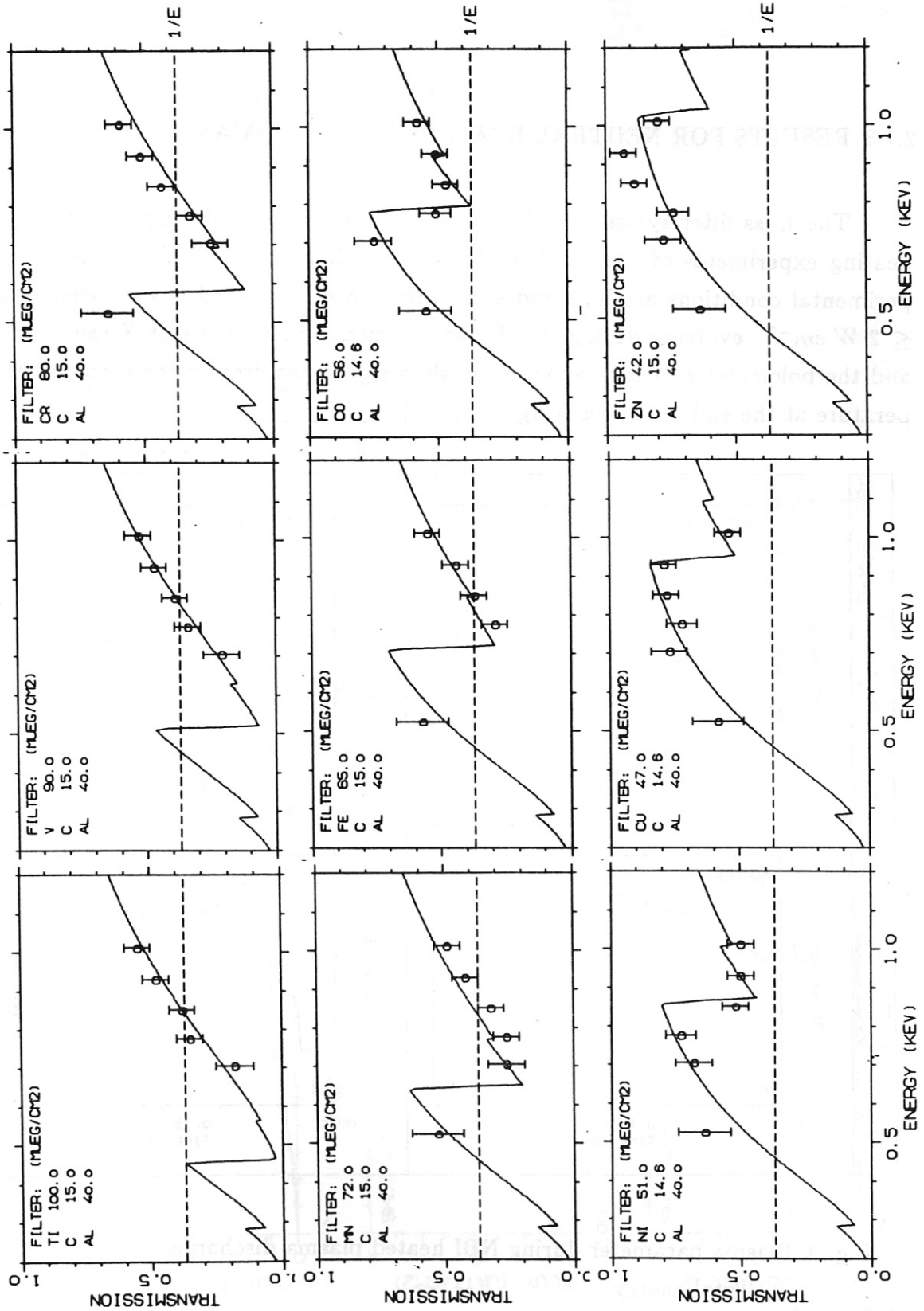


Fig. 3 Filter transmission curves for elements between Ti and Zn ; comparison of calculated transmission curves with measured data points.

### 2.1.3 RESULTS FOR NEUTRAL BEAM HEATED PLASMAS

The Ross filter system could be used only temporarily during neutral beam heating experiments of "currentless" Stellarator plasmas. Typically for these experimental conditions are high radiation with centrally peaked power densities of $\leq 2\ W\ cm^{-3}$ evolving during the discharge (measured by the soft X-ray camera and the bolometer system). Simultaneously a significant drop of the electron temperature at the end of the discharge occurrs [1-4].

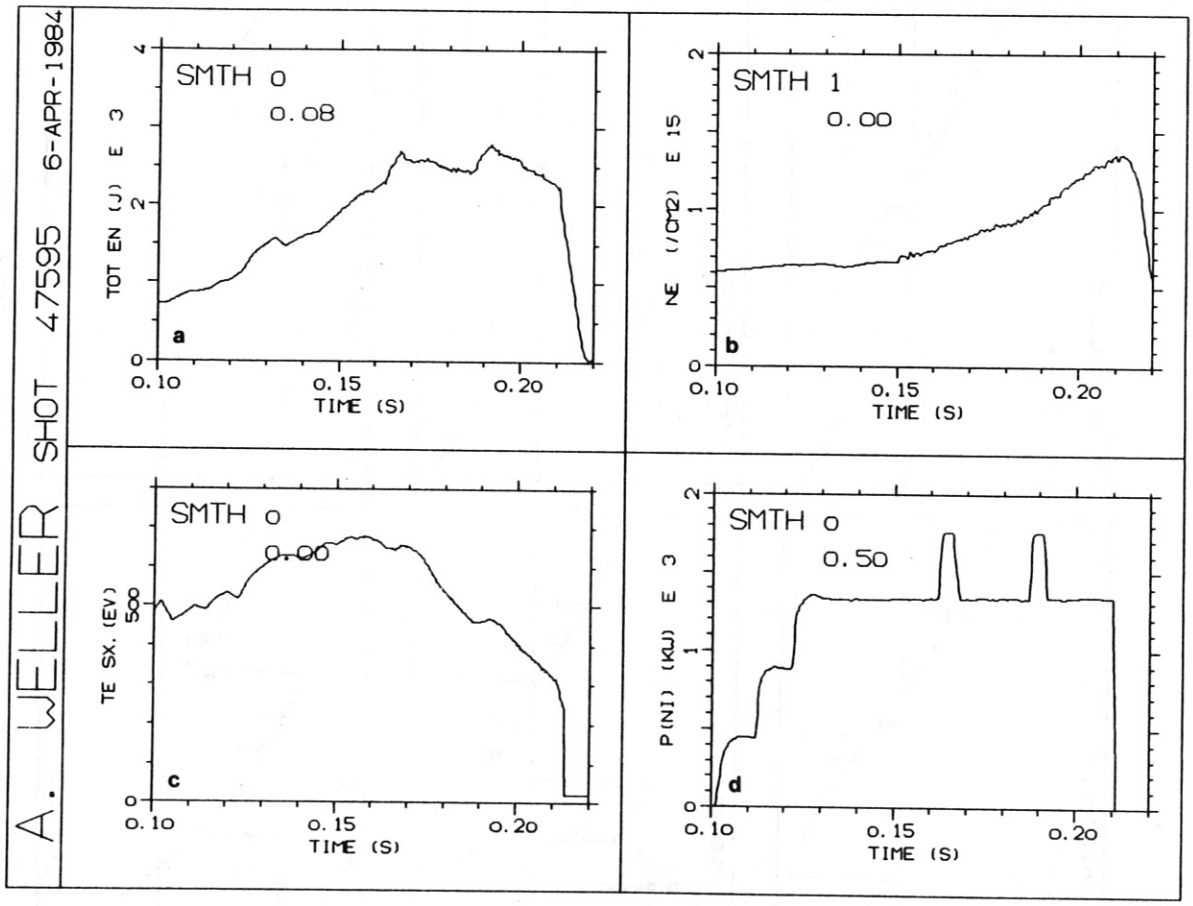


Fig. 4 Plasma parameter during NBI heated plasma discharge:

a) Total energy.

b) Line density.

c) Electron temperature (soft X filter method).

d) Injector power.

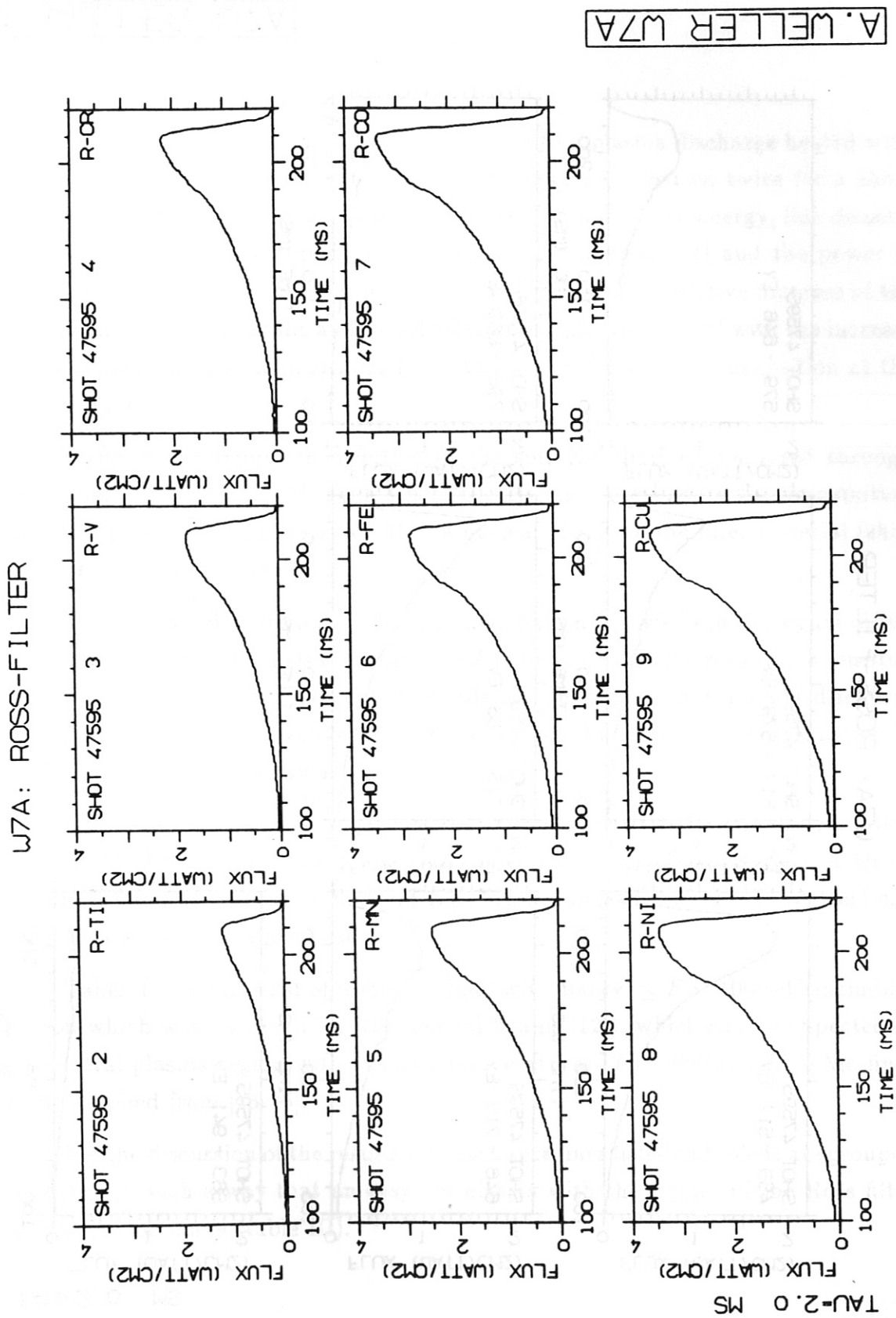


Fig. 5 Volume integrated soft X-ray intensity during NBI obtained through filters of Ti through Cu.

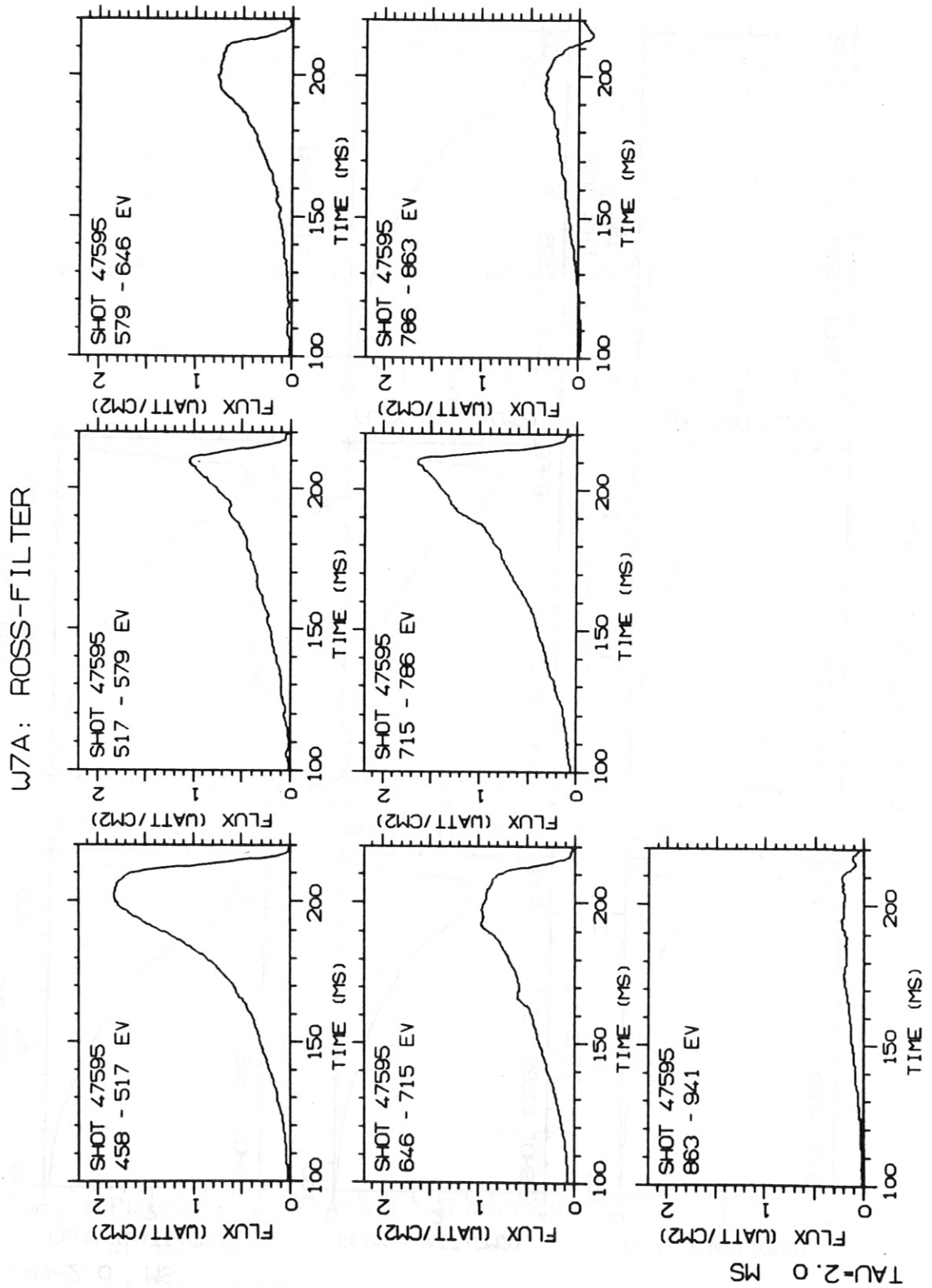


**Fig. 6** Soft X-ray intensity in different energy bands between $\sim$ 450 $eV$ and $\sim$ 940 $eV$.

A first example of the measurements refers to a plasma discharge heated with 3 neutral beam injectors with 1 additional injector switched on twice for a short time. Fig. 4 contains the basic plasma parameter (total stored energy, line density, central electron temperature from soft X-ray filter method [11] and the power of the neutral injectors) during application of NBI power. The relative increase of the plasma energy caused by the additional injector is higher compared with the increase of the central electron temperature indicating a significant power deposition at the plasma edge.

In fig. 5 the temporal evolution of the soft X-radiation monitored through the individual filters (Ti through Cu). Clearly, the intensity of the transmitted radiation progressively increases with the nuclear charge of the filter material (shift of the $L$ absorption edge).

The spectral distribution of the soft X-radiation follows from the signal differences between filter channels with adjacent $L$ edge energies. The resulting intensities corresponding to the different energy bands are plotted in fig. 6 for the discharge shown in figs. 4,5. The given intensities are corrected for the mean transmission in the individual energy channels.

As derived from earlier experiments, oxygen impurities from wall desorption and neutral beam contamination play a major role [1-4]. But also Fe, Cr (from vacuum vessel), Mo (from limiter and NBI beam dump plates) and Ti (getter) can contribute to the radiation losses.

Table II contains a list of resonance lines with $400\ eV \leq E \leq 1000\ eV$ (including carbon which was also found in the neutral beams [12]), which can be expected in the central plasma region with electron temperatures $T_e \leq 600\ eV$. The Mo-lines were compiled from [13-15].

For the discussion of the results the resonance lines listed in table II are grouped in energy in such a way that an easy correlation with the signals of the Ross filter system can be made (table III).

Table II

Prominent resonance lines contributing to radiation losses in the energy range 400 $eV \leq E \leq 1000\ eV$

| Ion | Transition | Wavelength [Å] | Transition energy [eV] |
|---|---|---|---|
| CVI | 1s → 3p | 28.5 | 436 |
| CVI | 1s → 4p | 27.0 | 459 |
| CVI | 1s → 5p | 26.4 | 471 |
| OVII | 1s → 2p | 21.6 | 574 |
| OVII | 1s → 2p | 21.8 | 569 |
| OVII | 1s → 3p | 18.6 | 667 |
| OVIII | 1s → 2p | 19.0 | 653 |
| OVIII | 1s → 3p | 16.0 | 775 |
| OVIII | 1s → 4p | 15.2 | 817 |
| OVIII | 1s → 5p | 14.8 | 837 |
| TiXIII | 2p → 4d | 19.2 | 646 |
| TiXIII | 2p → 4d | 19.4 | 640 |
| TiXIV | 2p → 3s | 24.3 | 510 |
| TiXIV | 2p → 3s | 24.7 | 501 |
| CrXV | 2p → 3d | 18.5 | 670 |
| CrXV | 2p → 3s | 21.2 | 586 |
| CrXV | 2p → 3s | 20.9 | 594 |
| CrXVI | 2p → 3d | 17.4 | 713 |
| CrXVI | 2p → 3s | 19.3 | 643 |
| CrXVI | 2p → 3s | 19.8 | 626 |
| FeXVII | 2p → 3d | 15.0 | 827 |
| FeXVII | 2p → 3s | 17.1 | 727 |
| FeXVII | 2p → 3s | 16.8 | 739 |
| FeXVIII | 2p → 3s | 16.0 | 774 |
| FeXVIII | 2p → 3d | 14.2 | 873 |
| MoXVIII | 3d → 4f | 29.5[a] | 420[a] |
| MoXIX | 3d → 4f | 27.5[a] | 450[a] |
| MoXX | 3d → 4f | 26.2[a] | 473[a] |
| MoXXI | 3d → 4f | 24.8[a] | 500[a] |
| MoXXII | 3d → 4f | 23.8[a] | 521[a] |

[a] mean value for transition array

Table III

Prominent resonance lines in filter transmission windows

| Filter pair | Energy window [eV] | Ion | Transition energy [eV] |
|---|---|---|---|
| Sc – Ti | 404 – 458 | CVI | 436 |
| | | MoXVIII | 420[a] |
| | | MoXIX | 450[a] |
| Ti – V | 458 – 517 | CVI | 459 |
| | | CVI | 471 |
| | | TiXIV | 510 |
| | | TiXIV | 501 |
| | | MoXX | 473[a] |
| | | MoXXI | 500[a] |
| V – Cr | 517 – 579 | OVII | 574 |
| | | OVII | 569 |
| | | MoXXII | 521[a] |
| Cr – Mn | 579 – 646 | TiXIII | 646 |
| | | TiXIII | 640 |
| | | CrXV | 586 |
| | | CrXV | 594 |
| | | CrXVI | 643 |
| | | CrXVI | 626 |
| Mn – Fe | 646 – 715 | OVII | 667 |
| | | OVIII | 653 |
| | | CrXV | 670 |
| | | CrXVI | 713 |
| Fe – Co | 715 – 786 | OVIII | 775 |
| | | FeXVII | 727 |
| | | FeXVII | 739 |
| | | FeXVIII | 774 |
| Co – Ni | 786 – 863 | OVIII | 817 |
| | | OVIII | 837 |
| | | FeXVII | 827 |
| Ni – Cu | 863 – 941 | FeXVIII | 873 |
| Cu – Zn | 941 – 1031 | | |

[a] mean value for transition array

The main conclusions, which can be drawn from fig. 6 and table III are:

- A large fraction of the radiation power is emitted in the range $458\ eV \leq E \leq 517\ eV$ which cannot be explained by oxygen or iron radiation. Mo or Ti are the most likely impurities which can produce this radiation. In the electron temperature region of typical NBI heated plasmas it is difficult to obtain a quantitative estimation of the Mo density from spectroscopic observation of few resonance lines because many lines are spread over an energy band (complicated transition arrays). Therefore, a significant radiation power may appear in the signals of the Ross filter system, whereas only a low radiation power may be contained in individual lines. Experimentally it has be shown by laser driven injection of Mo, that the surface barrier diodes can detect Mo-radiation in the low energy region ($E \leq 600\ eV$). On the other hand, Mo-line radiation around $2.5\ keV$ usually appears in the PHA-spectra of low density and high temperature plasmas. Crystal spectrometer measurements show no evidence of an important contribution of the Ti XIV-line at 24.3 Å. Since no significant power was found in the energy interval $404 - 458\ eV$ (not plotted), C VI-radiation should also be excluded.
- The intensity in the energy interval $786 - 863\ eV$, containing the strongest line of iron (Fe XVII at 15 Å), is relatively weak.
- The intensity in the energy interval $715 - 786\ eV$ is relatively high compared with the energy bands which should contain the strongest O VIII- and Fe XVII-lines.
- The time evolution of the intensities in the energy bands corresponding to the strongest O VII- and O VIII-lines shows the characteristic steeper increase at the end of the discharge for O VII compared with O VIII. In fig. 7 normalized intensities are compared with the signals of the crystal spectrometer (including also Fe XVII). The different behaviour of the O VII- and O VIII-radiation is a recombination effect at decreasing temperature. This is demonstrated in fig. 8 with the calculated power emissivity as a function of temperature in coronal equilibrium, which is a rather good approximation in the plasma centre, as transport simulations [3,4] have shown.

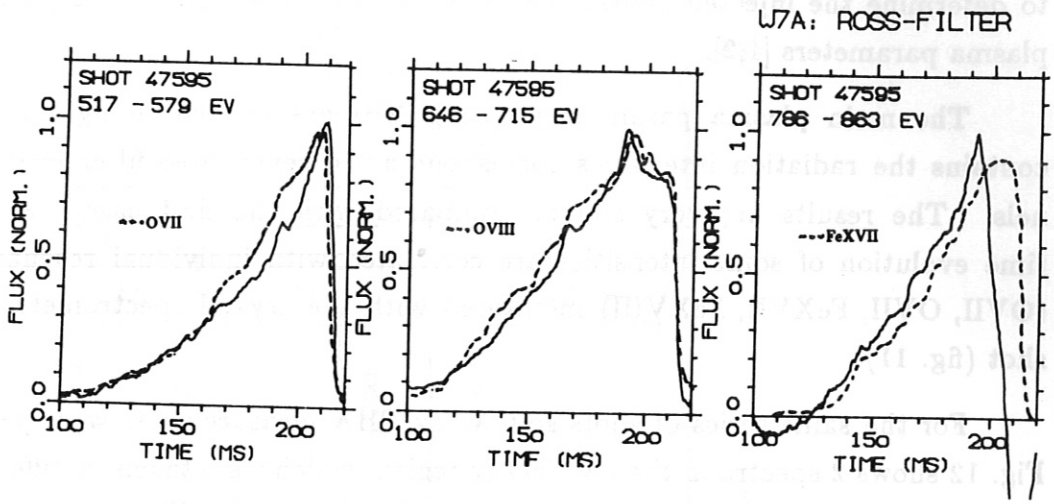


**Fig. 7** Comparison of normalized intensities in different energy bands with resonance lines (crystal spectrometer) of oygen and iron.

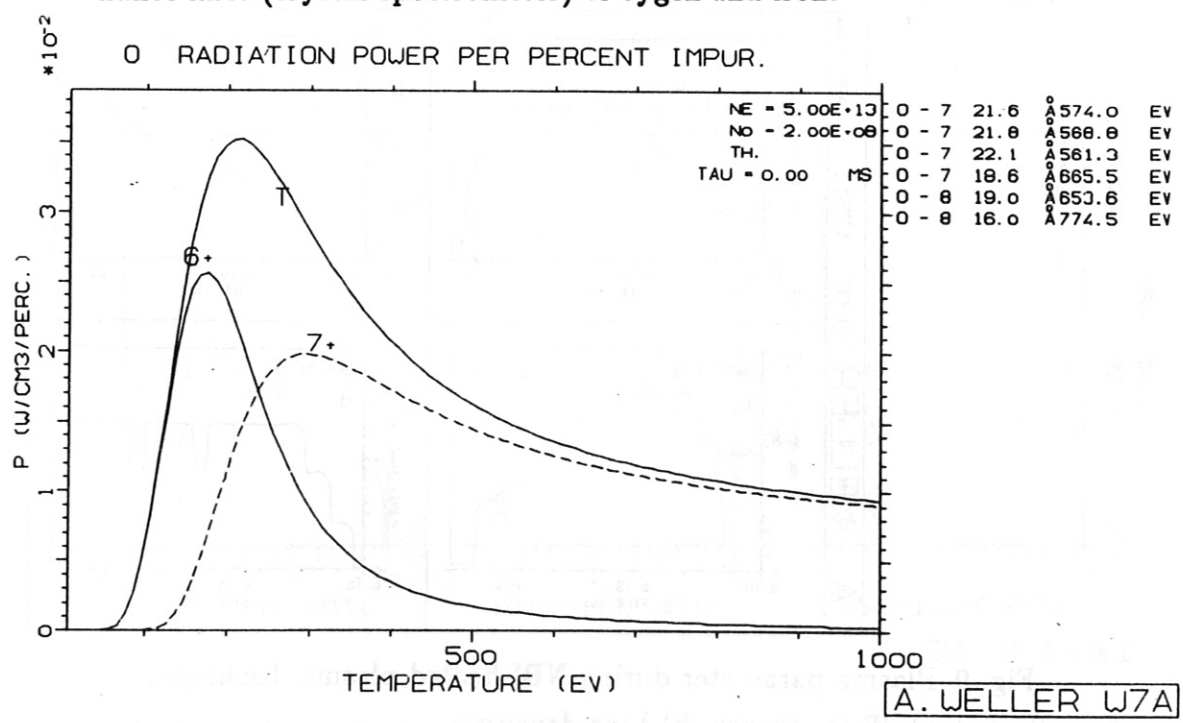


**Fig. 8** O VII-,O VIII radiation power in coronal equilibrium as functions of $T_e$.

A second example for analyzing the energy distribution of the soft X-radiation is given for a three injector discharge with the third injector switched off for a short time twice during the discharge. Switching on/off has been applied in order to determine the injected neutral beam power from the transient response of the plasma parameters [1,2].

The main plasma parameters during NBI are plotted in fig. 9. Fig. 10 contains the radiation intensities corresponding to seven Ross-filter energy channels. The results are very similar compared with the first case. Again, the time evolution of some intensities are correlated with individual resonance lines (OVII, OVII, FeXVII, FeXVIII) monitored with the crystal spectrometer shot by shot (fig. 11).

For the same series of shots soft X-ray PHA measurements were performed. Fig. 12 shows 2 spectra in the low energy region, which were taken in different time windows during about ten shots (energy resolution $\sim 200\ eV$).

The main radiation component is distributed in the range $\sim 550 - 700\ eV$ consistent with the Ross filter results, since the low energies are suppressed by the Si(Li)-diode.

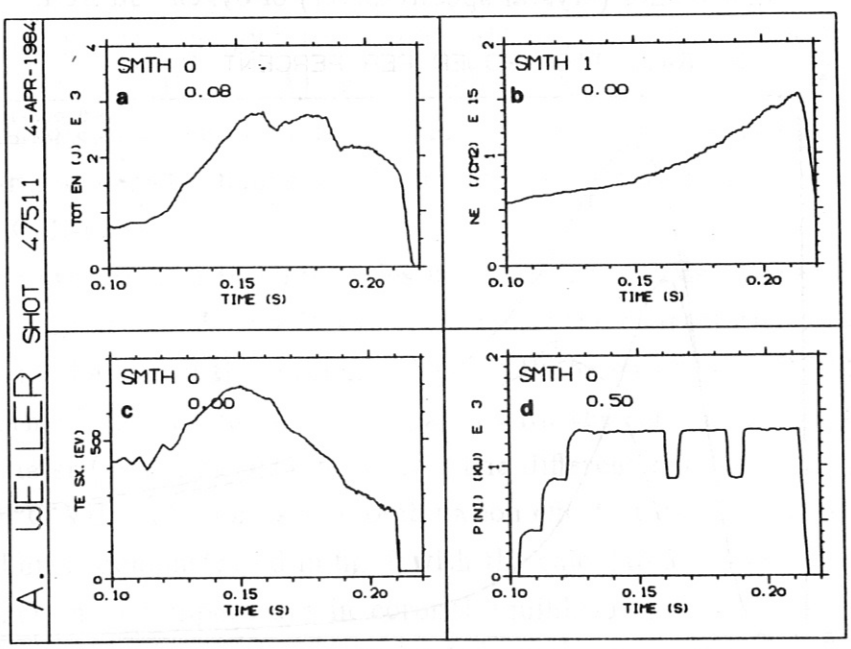


Fig. 9 Plasma parameter during NBI heated plasma discharge:

a) Total energy. b) Line density.

c) Electron temperature (soft X filter method).

d) Injector power.

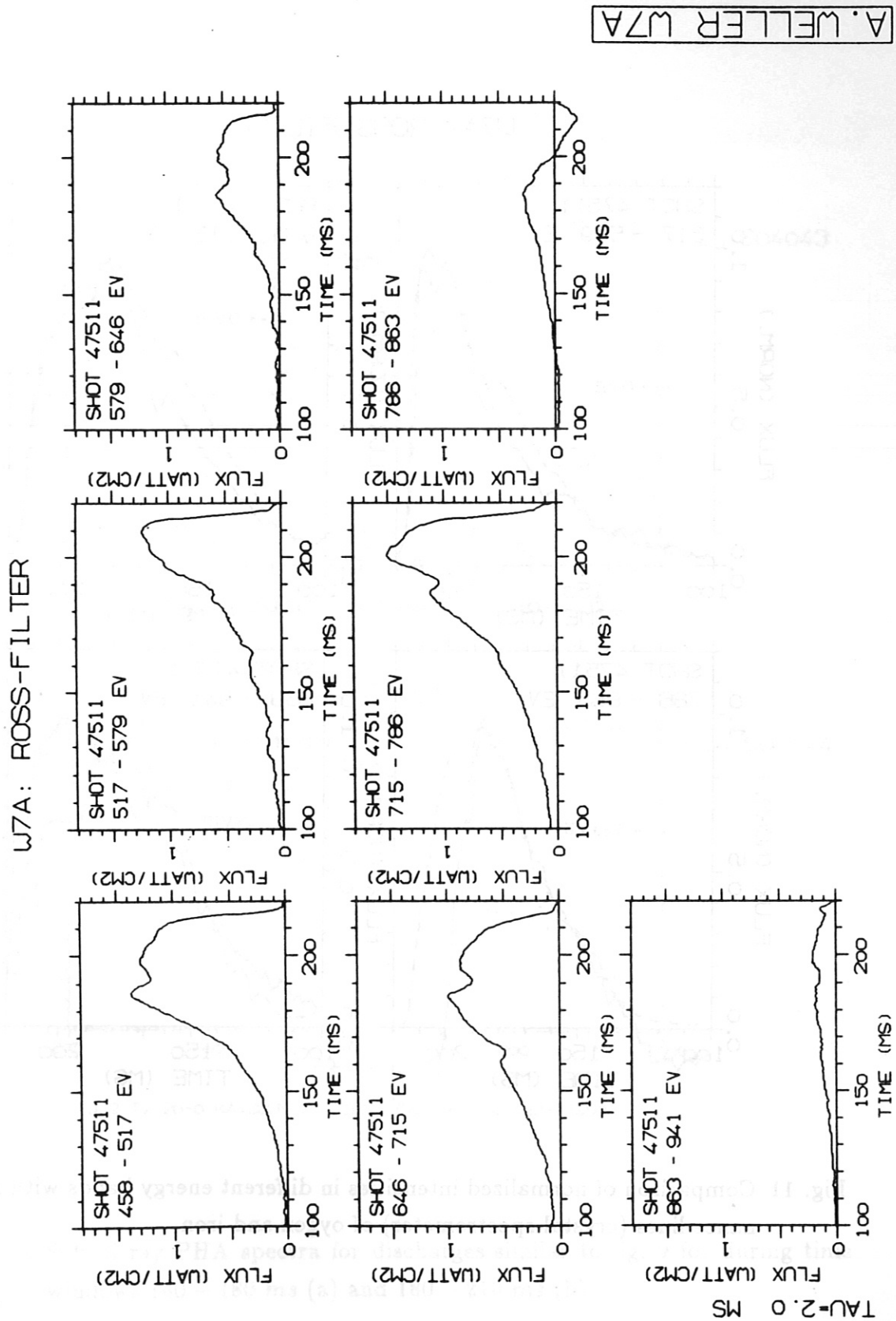


Fig. 10 Soft X-ray intensity in different energy bands between $\sim$ 450 $eV$ and $\sim$ 940 $eV$.

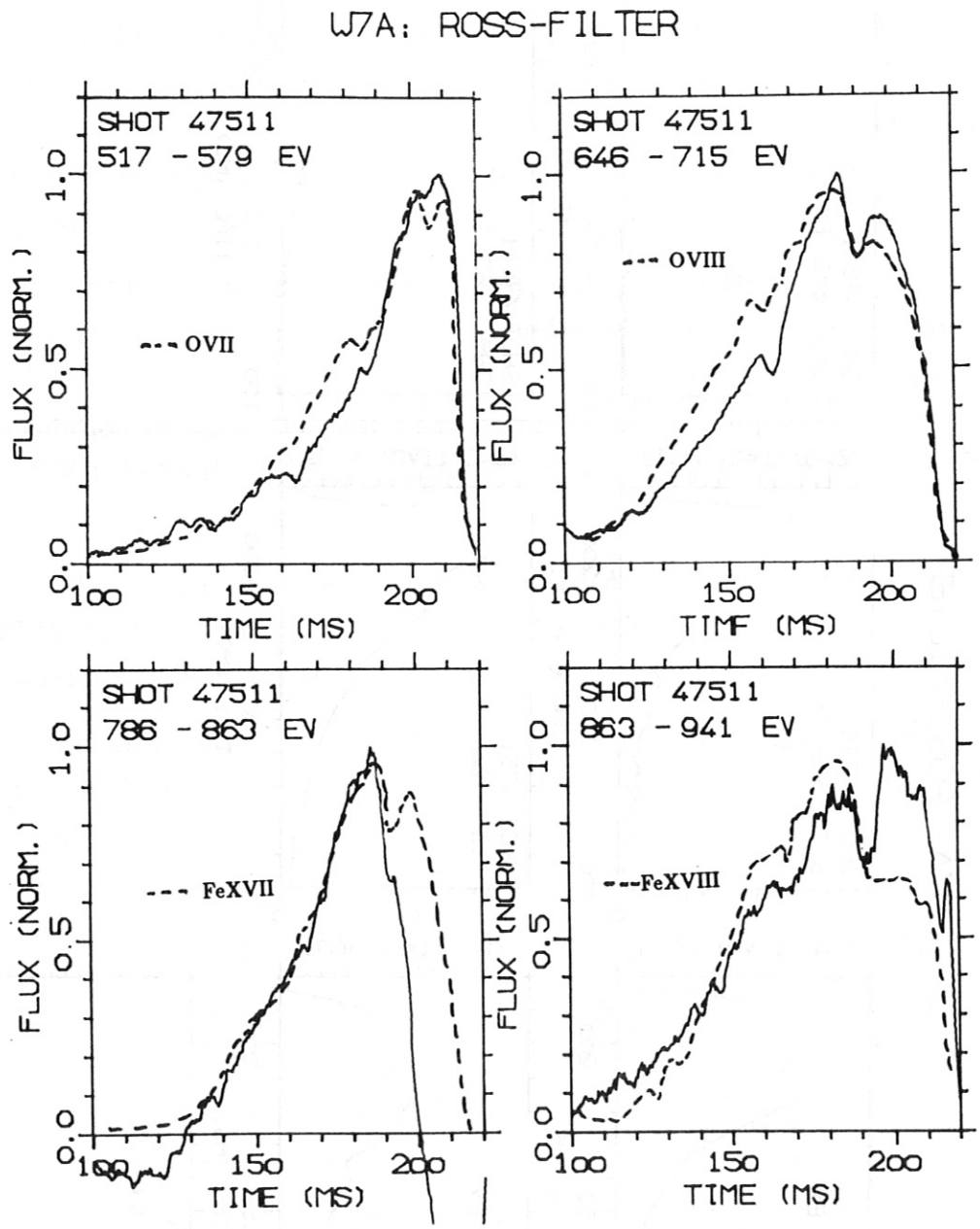


Fig. 11 Comparison of normalized intensities in different energy bands with resonance lines (crystal spectrometer) of oxygen and iron.

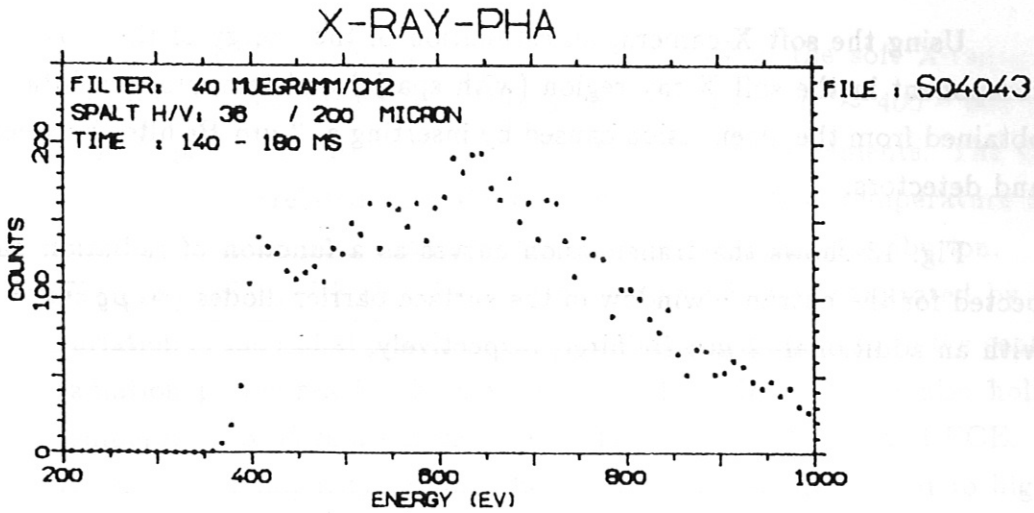


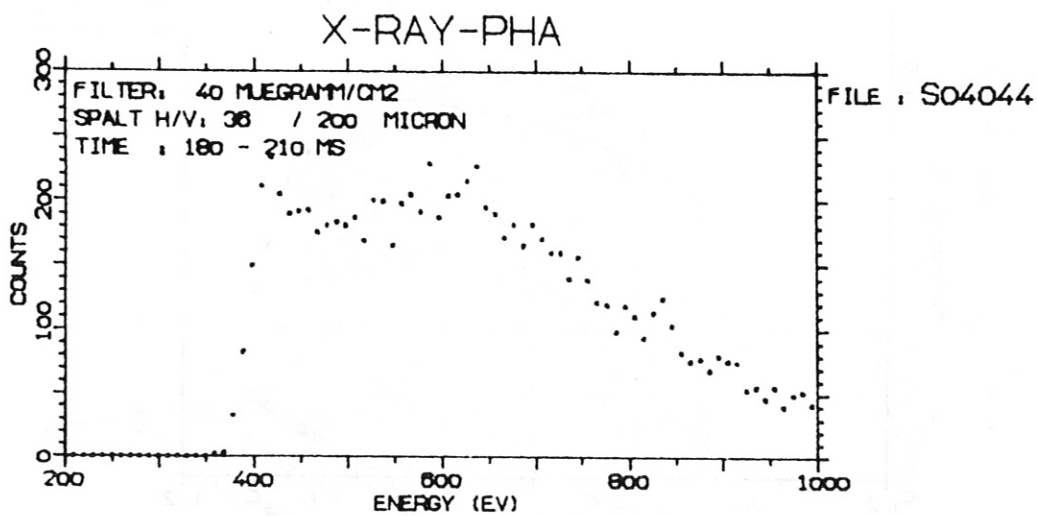


Fig. 12 Soft X-ray PHA spectra for discharges similar to fig. 9 for during time windows $140 - 180\ ms$ (a) and $180 - 210\ ms$ (b).

## 2.2. MEAN ENERGY FROM TWO FILTER MEASUREMENTS

Using the soft X-camera, an estimation of the energy of the most important component in the soft X-ray region (with spatial and temporal resolution) can be obtained from the attenuation caused by inserting a $2\ \mu m\ Be$ filter between plasma and detectors.

Fig. 13 shows the transmission curves as a function of radiation energy expected for the entrance window of the surface barrier diodes ($40\ \mu g\, cm^{-2}\ Al$ ) and with an additional $2\ \mu m\ Be$ filter, respectively.

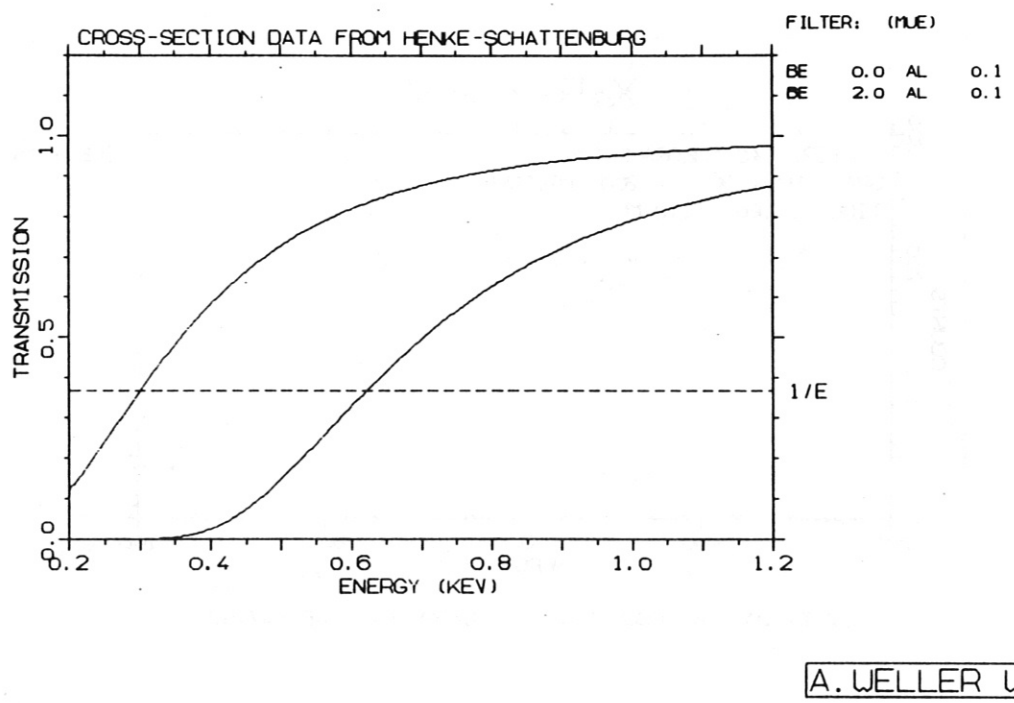


Fig. 13 Calculated energy response of surface barrier diodes without and with $2\ \mu m\ Be$ filter.

Some example of analyzing nearly identical shots without and with Be-filter are illustrated in the following:

- Fig. 14 gives the evolution of the mean energy of the soft X-radiation for typical shots during NBI. The values are between $\sim 400 - 600\ eV$ which again seems to be consistent with other measurements. The time variation is correlated with the change of the electron temperature and can be explained by a change of the charge state state distribution.
- The correlation with the electron temperature is also illustrated by the variation of the radial profiles, which can become hollow, when the central radiation power reaches high values (fig. 15). In this case also hollow temperature profiles are measured by Thomson scattering and ECE.
- By Ne tracer impurity puffing the radiation losses are shifted to higher energies, although the electron temperature decreases. This means, that the Ne line radiation around $\sim 1\ keV$ contributes to the total radiation (fig. 16 a without Ne, fig. 16 b with Ne).

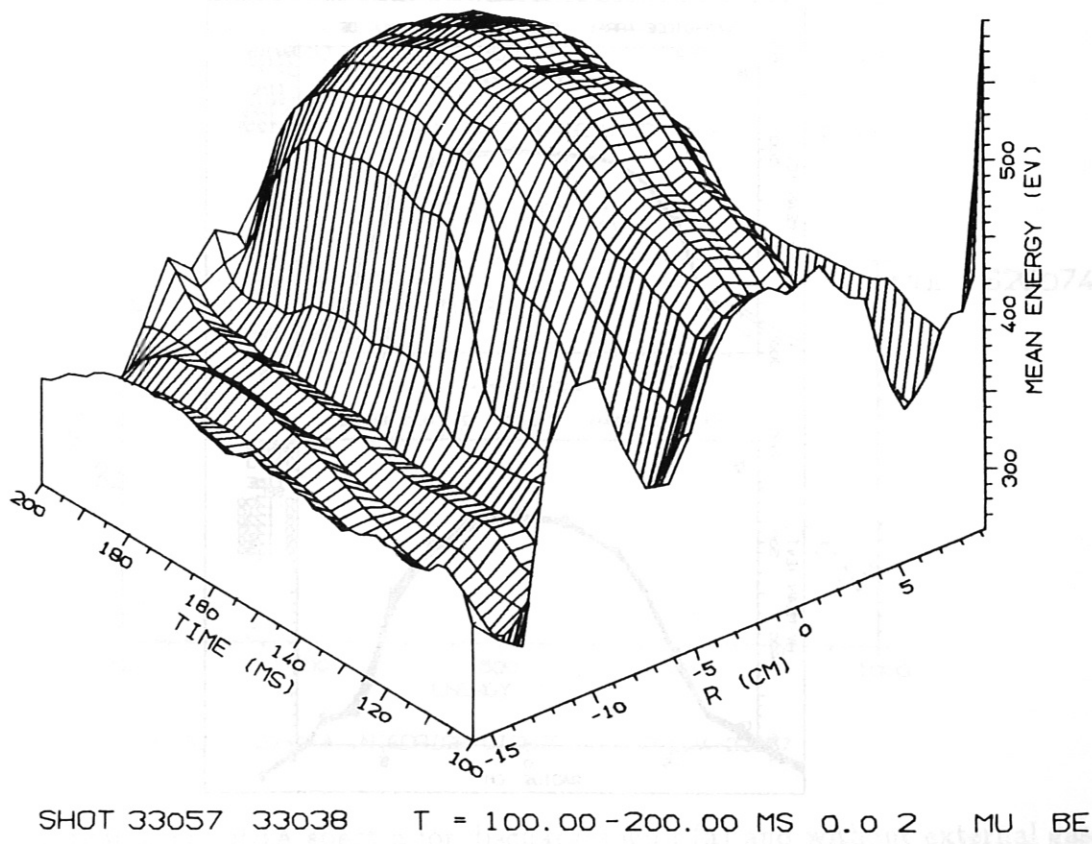


Fig. 14 Evolution of the mean energy of typical shots during NBI.

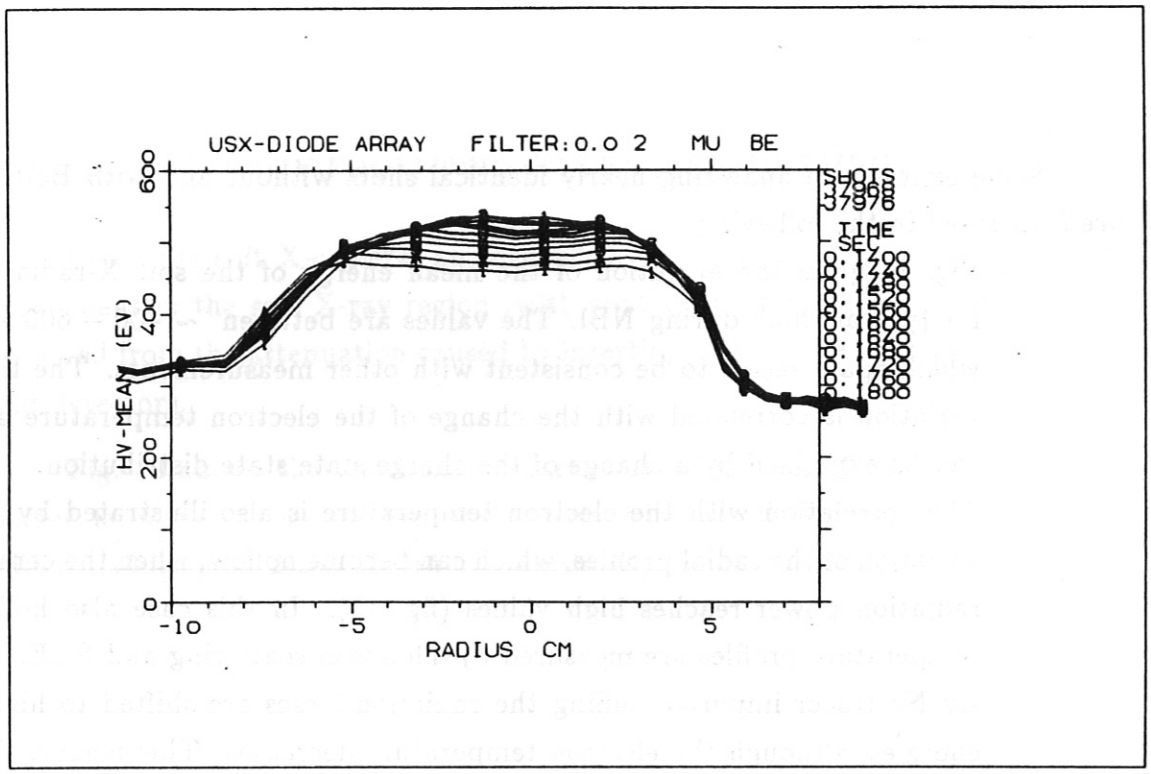


Fig. 15 Mean energy radial profiles during evolution of hollow $T_e$ profiles.

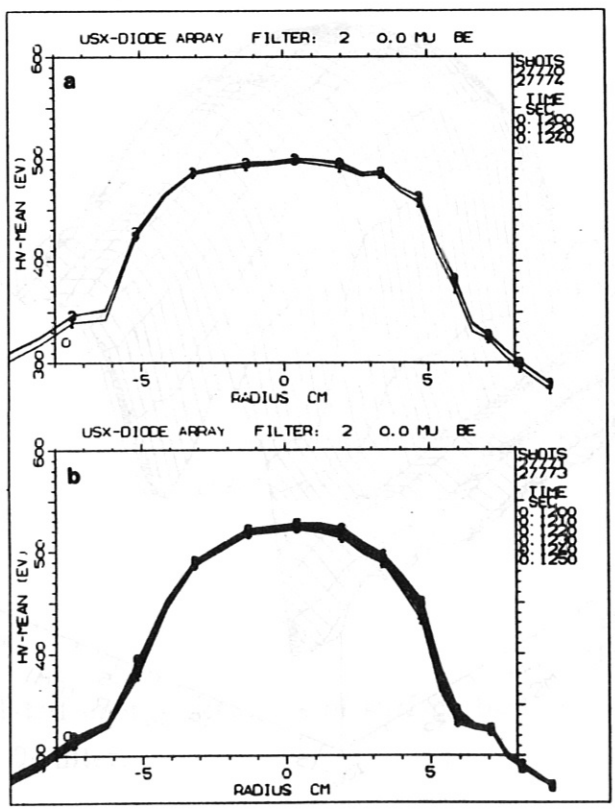


Fig. 16 Increase of the mean energy after Ne injection (b).

## 3. X-Ray Pulse Height Analysis

A 10 $mm^2$ windowless Si(Li)-detector was used to provide spectral information also in the energy region below $\sim 1\ keV$. A thin filter ($\sim 40\ \mu g\, cm^{-2}\ Al$ on a $\sim 15\ \mu g\, cm^{-2}\ C$ backing) served to remove the visible light. The energy resolution of the system is about $200\ eV$.

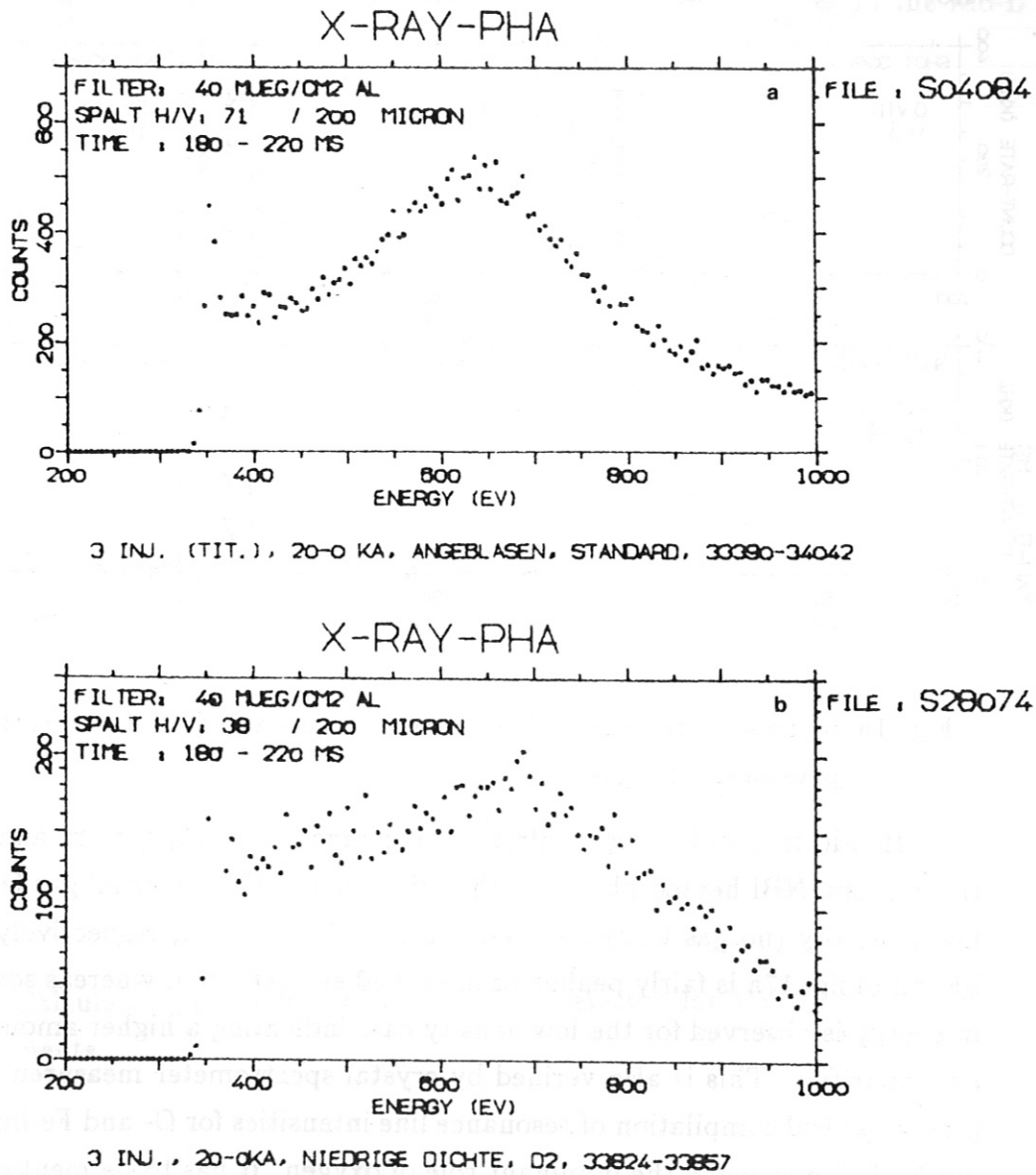


Fig. 17 Soft X-ray PHA spectra for discharges with (a) and without external gas feed (b).

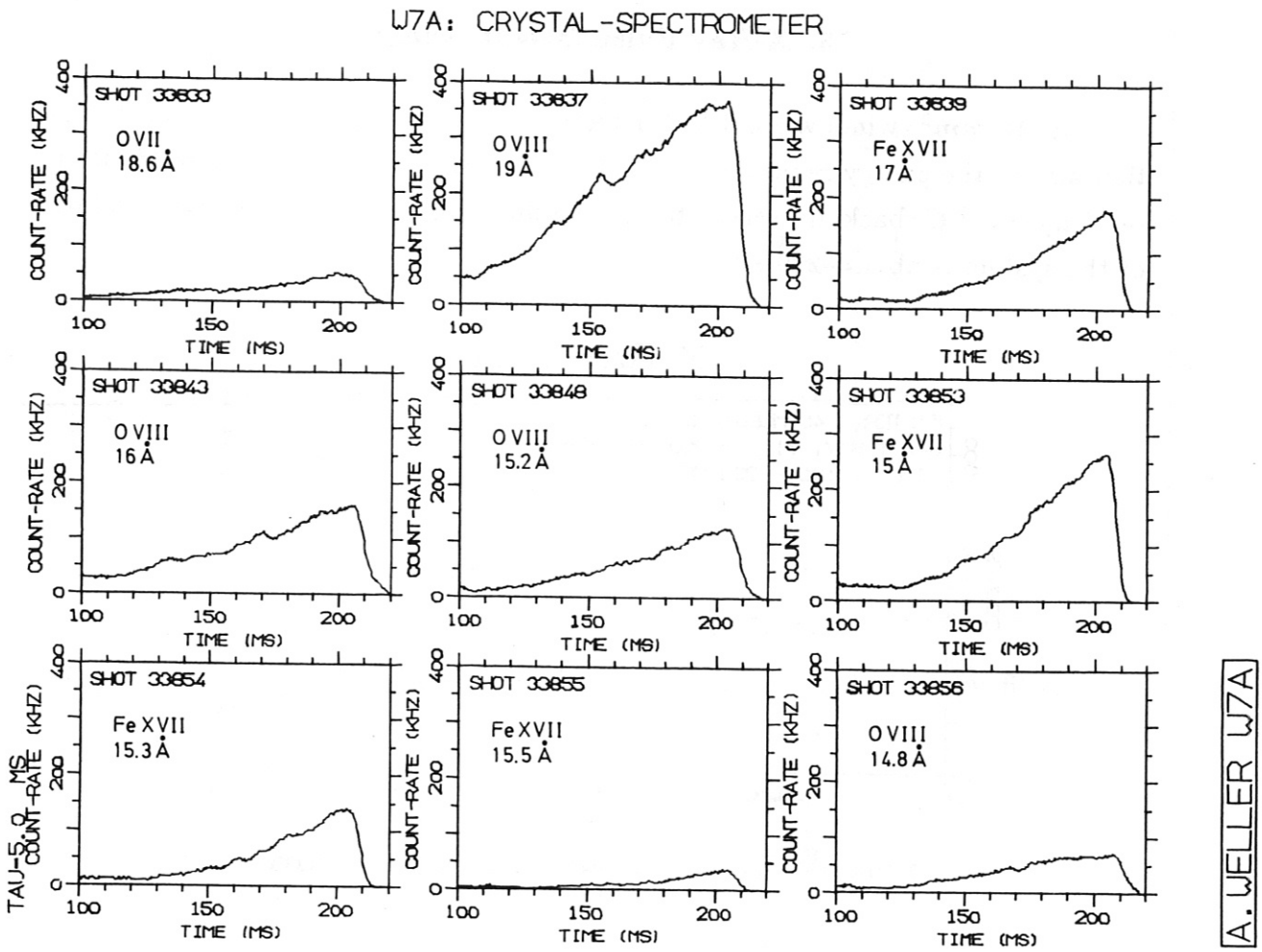


Fig. 18 Signals of resonance lines from oxygen and iron for a series of typical plasma discharges.

In addition to the result already presented in fig. 12, spectra analyzed during the end of a NBI heated plasma with high density (with external gas feed) and with lower density (no gas feed) are given in figs. 17a and 17b, respectively. The distribution of fig. 17a is fairly peaked around 650 $eV$ (O VIII), whereas some spreading in energy is observed for the low density case indicating a higher amount of Fe- and Cr-impurities. This is also verified by crystal spectrometer measurements. Fig. 18 gives a typical compilation of resonance line intensities for O- and Fe-impurities during NBI also showing the dominant role of oxygen. It has to be mentioned that the true intensities for the low energy lines are higher owing to the decreasing sensitivity of the detectors towards low energies. In fig. 19 the expected response function of the Si(Li)-diode including the transmission of the thin Al-filter is plotted.

Fig. 20 gives some examples of the detection of impurities by the observation of the energy region above $\sim 1\ keV$ . In this case a 50 $\mu m$ *Be* filter was applied (corresponding transmission curve plotted in fig. 21).

In fig. 20a the peak around $\sim 2.5\ keV$ indicates L-radiation from intrinsic Mo-impurties (ECRH heated plasma without NBI). Figs. 20b,c show the peaks of tracer impurity radiation (laser blow off of Al into NBI heated plasma [3,4] (20b), Kr gas puff into a ECRH heated plasma (20c)). In the latter case again the Mo-L line radiation appears in the spectrum.

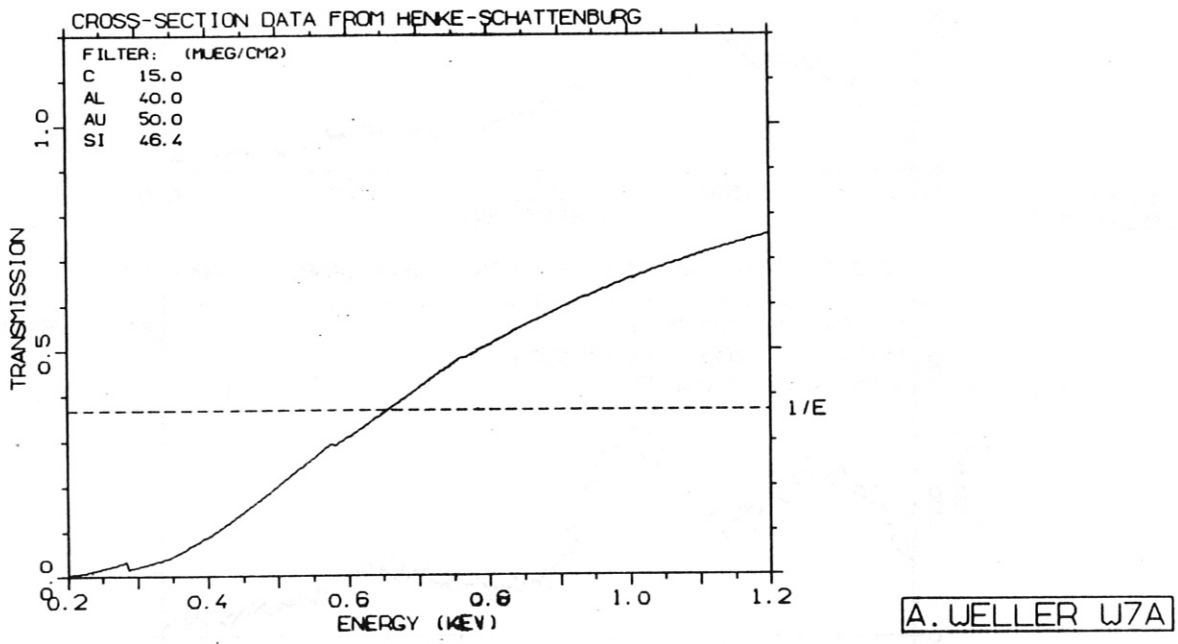


Fig. 19 Calculated energy response of Si(Li) detector for low energy measurements.

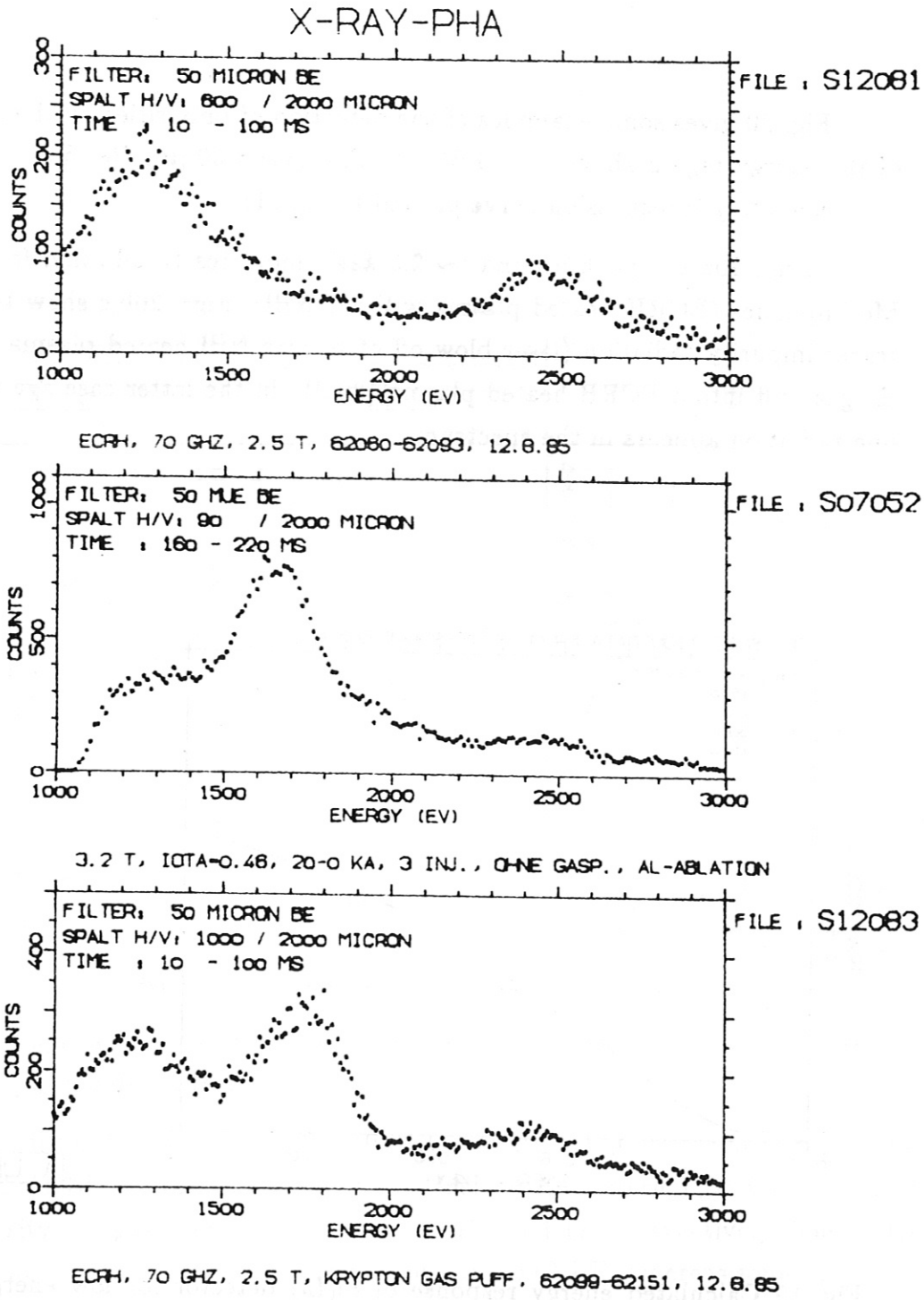


Fig. 20 a) PHA spectrum of ECRH heated plasma with Mo-L radiation at $\sim 2.5\ keV$.

b) PHA spectrum of NBI heated plasma with ALXII-radiation at $\sim 1.6\ keV$ after Al laser blow off.

c) PHA spectrum of ECRH heated plasma with Kr-lines at $\sim 1.75\ keV$ after Kr gas puffing.

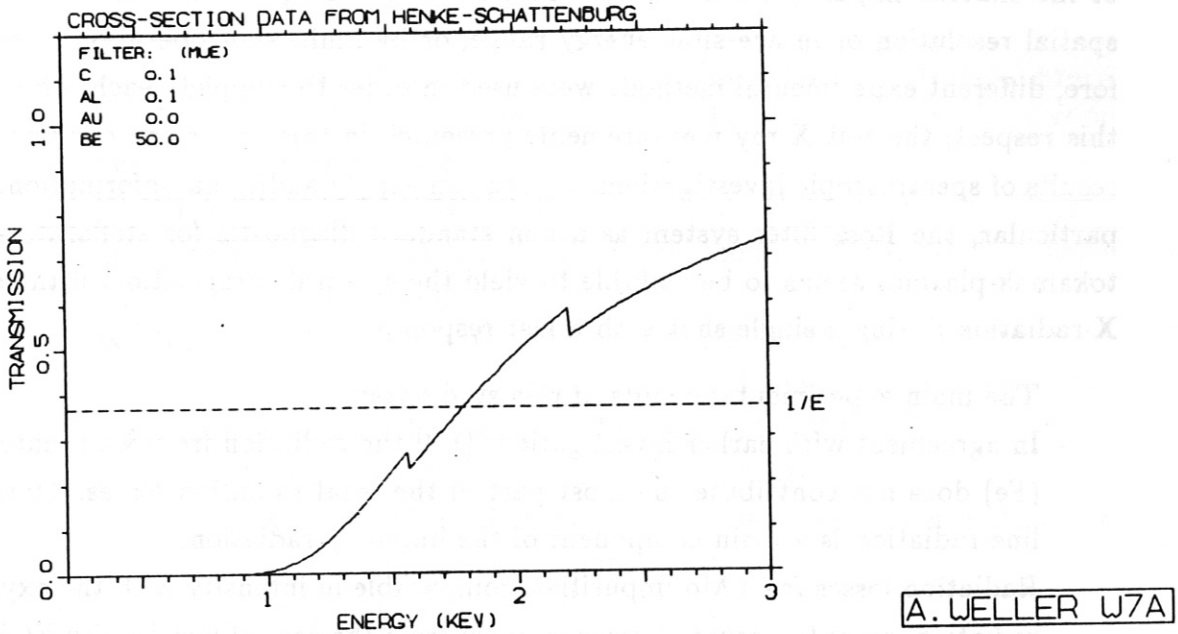


**Fig. 21** Calculated energy response of Si(Li) detector for measurements with the 50 $\mu m$ *Be* filter.

## 4. Summary

Almost all the diagnostics providing information about the energy spectrum of the emitted impurity radiation have limitations in energy or time resolution, in spatial resolution or in acessible energy range, or by multi shot operation. Therefore, different experimental methods were used in order to complete each other. In this respect, the soft X-ray measurements presented in this paper can confirm the results of spectroscopic investigations or even can supply additional information. In particular, the Ross filter system as a non standard diagnostic for stellarator- or tokamak-plasmas seems to be suitable to yield the spectral composition of the soft X-radiation during a single shot with a fast response.

The main experimental results of this study are:

- In agreement with earlier investigations [1-4] the radiation from wall material (Fe) does not contribute the most part of the total radiation losses. Oxygen line radiation is a main component of the impurity radiation.
- Radiation losses from Mo-impurities, comparable in intensity with the oxygen radiation, seem to occurr. However, apart from the case of low density ECRH-heated plasmas, no direct proof was available.

In addition to the investigation of the intrinsic impurity radiation, the application of Ross filters should be particularly suitable to monitor the radial and temporal evolution of tracer impurities. Also the analysis of the continuum radiation intensity in energy bands free of resonance line radiation should be possible in order to get $Z_{eff}$ or $T_e$.


## Acknowledgements

The excellent work of D. Gonda with respect to the experimental setup and his contributions to the measurements is gratefully acknowledged. The author is also indebted to Dr. P. Maier-Komor and Mrs. K. Nacke (TU München) for the preparation of the X-ray filters. The author thanks Dr. H. Hacker for his contributions with respect of the crystal spectrometer measurements and for many discussions of the results. Special thanks also to Dr. P. Smeulders, who initiated the two filter measurements.

## References


[1] W VII-A TEAM, NI GROUP, Proc. 9th Int. Conf. on Plasma Physics and Controlled Nuclear Fusion Research, Baltimore 1982, Nucl. Fusion Suppl., Vol. 2, (1983) 241

[2] W VII-A TEAM, NI GROUP, Proc. 10th Int. Conf. on Plasma Physics and Controlled Nuclear Fusion Research, London 1984, Nucl. Fusion Suppl., Vol. 2, (1985) 371

[3] W VII-A TEAM, NI GROUP, Proc. 10th Int. Conf. on Plasma Physics and Controlled Nuclear Fusion Research, London 1984, Nucl. Fusion Suppl., Vol. 2, (1985) 635

[4] W VII-A TEAM, NI GROUP, Nuclear Fusion 25 No. 11 (1985)

[5] ROSS, P.A., J. Opt. Soc. Amer. and Rev. Sci. Instrum. 16 (1928) 433

[6] VAN PAASSEN, H.L.L., Rev. Sci. Instrum. 42 (1971) 1823

[7] JOHNSON, D.J., Rev. Sci. Instrum. 45 (1974) 191

[8] HENKE, B.L., SCHATTENBURG, M.L., Advances in X-Ray Analysis, Vol. 19, Plenum Press, New York (1976) 749

[9] VEIGELE, W.J., Atomic Data tables 5 (1973) 51

[10] W VII-A Team, Mode and sawtooth behaviour during neutral beam injection in the W VII-A Stellarator, Max-Planck-Institut für Plasmaphysik Garching, Rep. IPP 2/250 (1980).

[11] SMEULDERS, P., Soft X-ray fluxes as a diagnostic for hot plasmas, Max-Planck-Institut für Plasmaphysik Garching, Rep. IPP 2/233 (1979).

[12] OTT, W., FREUDENBERGER, K., PENNINGSFELD, F.P., PROBST, F., SÜSS, R., Rev. Sci. Instrum. 54 (1983) 50

[13] BRETON, C., DE MICHELIS, C., FINKENTHAL, M., MATTIOLI, M., Line emission from TFR 600 Plasmas in the spectral region 10 – 300 Å, CEA Fontenay aux Roses, Rep. EUR-CEA-FC-1039 (1980).

[14] BRETON, C., DE MICHELIS, C., FINKENTHAL, M., MATTIOLI, M., Ionization equilibrium of selected elements from Neon to Tungsten of interest in Tokamak plasma research, CEA Fontenay aux Roses, Rep. EUR-CEA-FC-948 (1978).

[15] SCHWOB, J.L., KLAPISCH, M., FINKENTHAL, M., SCHWEITZER, N., T.F.R. GROUP, Identification of Mo XV to Mo XXXIII in the soft X-ray spectrum of the TFR Tokamak, CEA Fontenay aux Roses, Rep. EUR-CEA-FC-887 (1977).